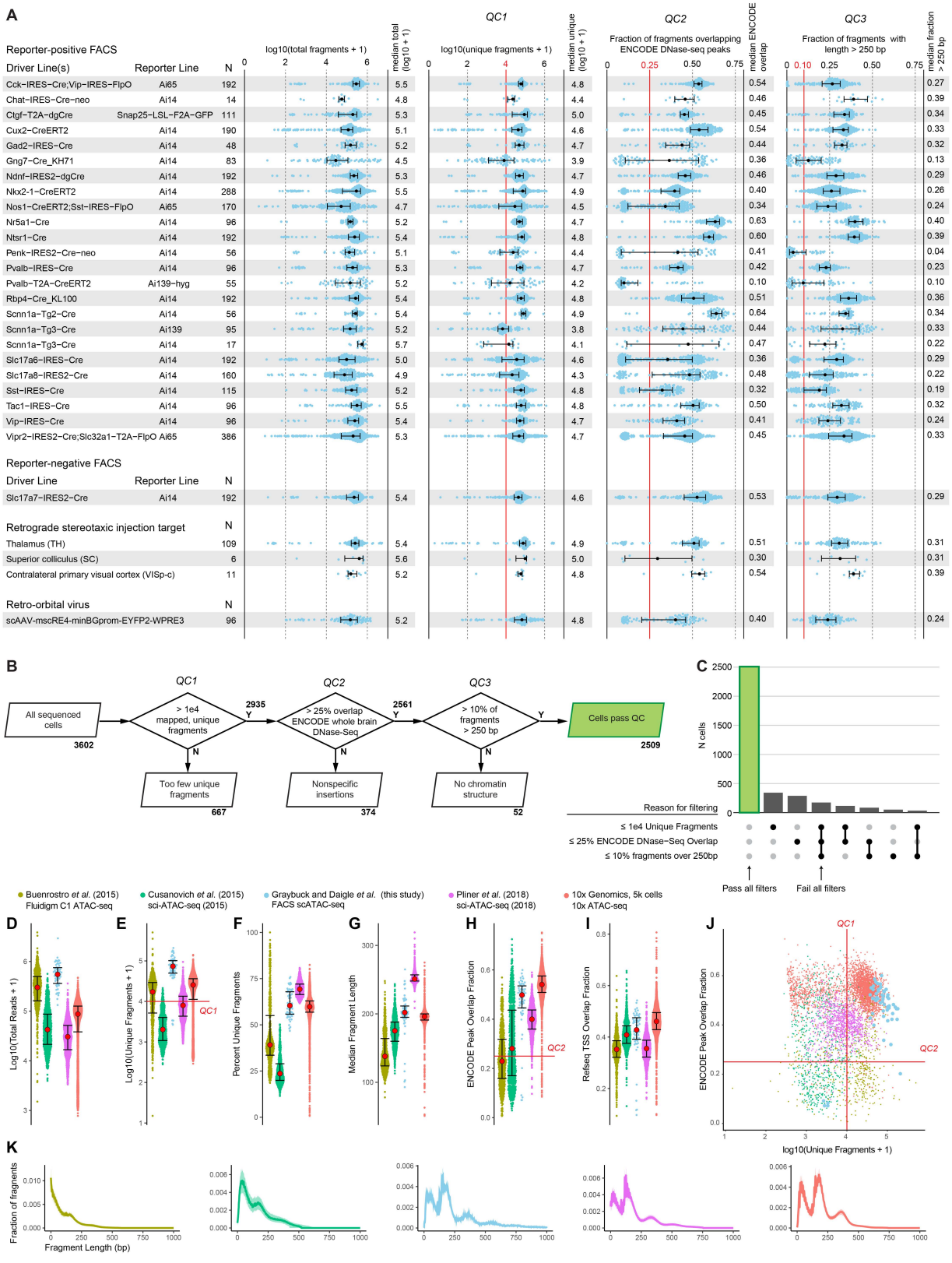
A
Reporter-positive FACS
Driver Line(s)
Reporter Line
N
log10(total fragments + 1)
median total (log10 + 1)
QC1
log10(unique fragments + 1)
median unique (log10 + 1)
QC2
Fraction of fragments overlapping ENCODE DNase-seq peaks
median ENCODE overlap
QC3
Fraction of fragments with length > 250 bp
median fraction > 250 bp
Cck−IRES−Cre;Vip−IRES−FlpO Ai65 192 5.5 4.8 0.54 0.27
Chat−IRES−Cre−neo Ai14 14 4.8 4.4 0.46 0.39
Ctgf−T2A−dgCre Snap25−LSL−F2A−GFP 111 5.3 5.0 0.45 0.34
Cux2−CreERT2 Ai14 190 5.1 4.6 0.54 0.33
Gad2−IRES−Cre Ai14 48 5.2 4.7 0.44 0.32
Gng7−Cre_KH71 Ai14 83 4.5 3.9 0.36 0.13
Ndnf−IRES2−dgCre Ai14 192 5.3 4.7 0.46 0.29
Nkx2−1−CreERT2 Ai14 288 5.5 4.9 0.40 0.26
Nos1−CreERT2;Sst−IRES−FlpO Ai65 170 4.7 4.5 0.34 0.24
Nr5a1−Cre Ai14 96 5.2 4.7 0.63 0.40
Ntsr1−Cre Ai14 192 5.4 4.8 0.60 0.39
Penk−IRES2−Cre−neo Ai14 56 5.1 4.4 0.41 0.04
Pvalb−IRES−Cre Ai14 96 5.3 4.7 0.42 0.23
Pvalb−T2A−CreERT2 Ai139−hyg 55 5.2 4.2 0.10 0.10
Rbp4−Cre_KL100 Ai14 192 5.4 4.8 0.51 0.36
Scnn1a−Tg2−Cre Ai14 56 5.4 4.9 0.64 0.34
Scnn1a−Tg3−Cre Ai139 95 5.2 3.8 0.44 0.33
Scnn1a−Tg3−Cre Ai14 17 5.7 4.1 0.47 0.22
Slc17a6−IRES−Cre Ai14 192 5.0 4.6 0.36 0.29
Slc17a8−IRES2−Cre Ai14 160 4.9 4.3 0.48 0.22
Sst−IRES−Cre Ai14 115 5.2 4.8 0.32 0.19
Tac1−IRES−Cre Ai14 96 5.5 4.8 0.50 0.32
Vip−IRES−Cre Ai14 96 5.4 4.7 0.41 0.24
Vipr2−IRES2−Cre;Slc32a1−T2A−FlpO Ai65 386 5.3 4.7 0.45 0.33
Reporter-negative FACS
Driver Line
Reporter Line
N
Slc17a7−IRES2−Cre Ai14 192 5.4 4.6 0.53 0.29
Retrograde stereotaxic injection target
N
Thalamus (TH) 109 5.4 4.9 0.51 0.31
Superior colliculus (SC) 6 5.6 5.0 0.30 0.31
Contralateral primary visual cortex (VISp-c) 11 5.2 4.8 0.54 0.39
Retro-orbital virus
N
scAAV-mscRE4-minBGprom-EYFP2-WPRE3 96 5.2 4.8 0.40 0.24
B
QC1
QC2
QC3
All sequenced cells
3602
> 1e4 mapped, unique fragments
2935
Y
N
Too few unique fragments
667
> 25% overlap ENCODE whole brain DNase-Seq
2561
Y
N
Nonspecific insertions
374
> 10% of fragments > 250 bp
Y
N
No chromatin structure
52
Cells pass QC
2509
C
N cells
Reason for filtering
≤ 1e4 Unique Fragments
≤ 25% ENCODE DNase−Seq Overlap
≤ 10% fragments over 250bp
Pass all filters
Fail all filters
Buenrostro et al. (2015) Fluidigm C1 ATAC-seq
Cusanovich et al. (2015) sci-ATAC-seq (2015)
Graybuck and Daigle et al. (this study) FACS scATAC-seq
Pliner et al. (2018) sci-ATAC-seq (2018)
10x Genomics, 5k cells 10x ATAC-seq
D
Log10(Total Reads + 1)
E
Log10(Unique Fragments + 1)
QC1
F
Percent Unique Fragments
G
Median Fragment Length
H
ENCODE Peak Overlap Fraction
QC2
I
Refseq TSS Overlap Fraction
J
QC1
QC2
ENCODE Peak Overlap Fraction
log10(Unique Fragments + 1)
K
Fraction of fragments
Fragment Length (bp)

Figure S1. Cell sources, QC Statistics, and comparisons to previously published methods, related to Figure 2. (**A**) Fragment number and quality for each cell source in the scATAC-seq dataset. See **Table S1** for mouse line details. N, number of cells collected. 'Total fragments' is the count of all sequenced fragments for each cell. 'Unique fragments' is the number of uniquely-mapped fragments and was used for the first QC cutoff of (> 10,000 unique fragments; QC1). Fraction of fragments overlapping ENCODE DNase-seq peaks was computed for uniquely mapped fragments and was used for the second QC cutoff (> 0.25; QC2). Fraction of fragments with length > 250 bp was computed for unique fragments and was used for the third QC cutoff of (> 0.1; QC3). (**B**) Flow chart showing how many samples were sequentially filtered by these three QC criteria. (**C**) Set barplot showing how many cells were flagged with each combination of QC criteria. (**D-K**) Comparison of FACS scATAC-seq libraries to those previously generated using Fluidigm C1 (Buenrostro et al., 2015), sci-ATAC-seq (Cusanovich et al., 2015; Pliner et al., 2018), or droplet-based indexing (10x Genomics) for which data using the common cell line of human GM12878 cells is available. To use in these comparisons, we generated scATAC-seq data using our FACS-based method for 60 GM12878 cells. For each published dataset, raw data was obtained from GEO and was aligned and analyzed using the same methods. For 10x Genomics, aligned fragment locations and metadata were obtained from the 10x genomics website for the "5k 1:1 mixture of fresh frozen human (GM12878) and mouse (A20) cells" dataset. Only samples labeled as GM12878 in sample metadata for each dataset were used for analysis. The color key above panels (D-I) are used throughout the plots (D) Beeswarm plots showing the total reads per cell. For all similar plots (A-F), each point represents a single cell, with bars showing the 25th and 75th percentiles, and central red dots showing the median values. (E) Number of uniquely mapped fragments per cell for each dataset. (F) Percent uniquely mapped fragments for each dataset. A high fraction of unique fragments (as in Pliner *et al.*) suggests that deeper sequencing will yield additional useful data. (G) Median fragment length for each dataset. (H) Fraction of reads overlapping ENCODE DNase-seq data generated for GM12878 cells. (I) Fraction of reads overlapping RefSeq TSS regions (TSS ± 5kb) for each dataset. (J) Two-axis QC criteria plot, as in **Fig. 2**, showing the QC1 and QC2 cutoffs used for mouse cortical scATAC-seq data. (**K**) Aggregate fragment length frequency plots. Fragment length is shown on the x-axis, and the fraction of reads with fragments of each bp size was calculated for each sample in each dataset. For this analysis, the median fraction at each fragment size is shown as a solid line, with 25th and 75th percentiles shown as shaded regions.

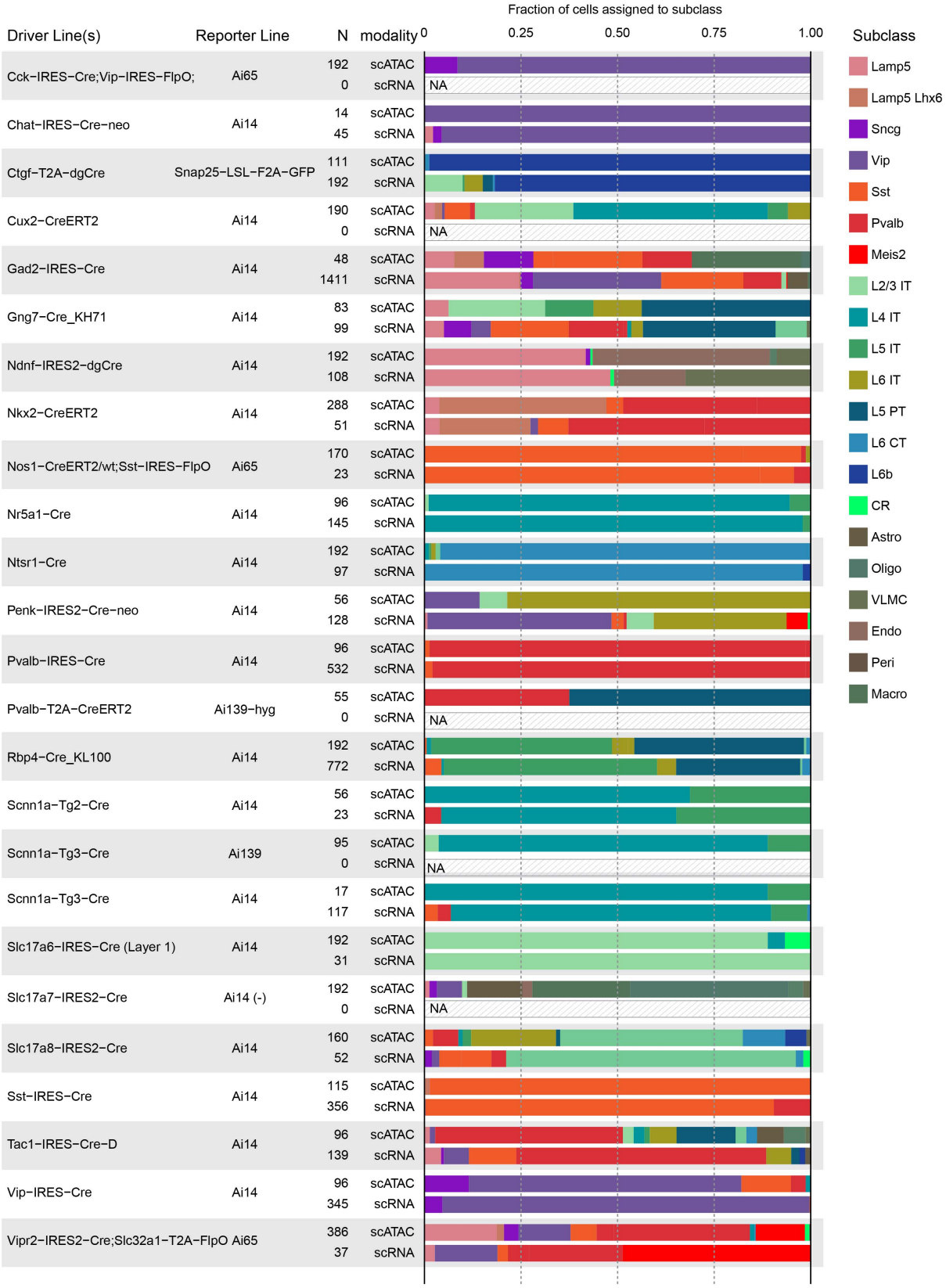
Fraction of cells assigned to subclass
0
0.25
0.50
0.75
1.00
Driver Line(s)
Reporter Line
N
modality
Cck−IRES−Cre;Vip−IRES−FlpO;
Ai65
192
scATAC
0
scRNA
NA
Chat−IRES−Cre−neo
Ai14
14
scATAC
45
scRNA
Ctgf−T2A−dgCre
Snap25−LSL−F2A−GFP
111
scATAC
192
scRNA
Cux2−CreERT2
Ai14
190
scATAC
0
scRNA
NA
Gad2−IRES−Cre
Ai14
48
scATAC
1411
scRNA
Gng7−Cre_KH71
Ai14
83
scATAC
99
scRNA
Ndnf−IRES2−dgCre
Ai14
192
scATAC
108
scRNA
Nkx2−CreERT2
Ai14
288
scATAC
51
scRNA
Nos1−CreERT2/wt;Sst−IRES−FlpO
Ai65
170
scATAC
23
scRNA
Nr5a1−Cre
Ai14
96
scATAC
145
scRNA
Ntsr1−Cre
Ai14
192
scATAC
97
scRNA
Penk−IRES2−Cre−neo
Ai14
56
scATAC
128
scRNA
Pvalb−IRES−Cre
Ai14
96
scATAC
532
scRNA
Pvalb−T2A−CreERT2
Ai139−hyg
55
scATAC
0
scRNA
NA
Rbp4−Cre_KL100
Ai14
192
scATAC
772
scRNA
Scnn1a−Tg2−Cre
Ai14
56
scATAC
23
scRNA
Scnn1a−Tg3−Cre
Ai139
95
scATAC
0
scRNA
NA
Scnn1a−Tg3−Cre
Ai14
17
scATAC
117
scRNA
Slc17a6−IRES−Cre (Layer 1)
Ai14
192
scATAC
31
scRNA
Slc17a7−IRES2−Cre
Ai14 (-)
192
scATAC
0
scRNA
NA
Slc17a8−IRES2−Cre
Ai14
160
scATAC
52
scRNA
Sst−IRES−Cre
Ai14
115
scATAC
356
scRNA
Tac1−IRES−Cre−D
Ai14
96
scATAC
139
scRNA
Vip−IRES−Cre
Ai14
96
scATAC
345
scRNA
Vipr2−IRES2−Cre;Slc32a1−T2A−FlpO
Ai65
386
scATAC
37
scRNA
Subclass
Lamp5
Lamp5 Lhx6
Sncg
Vip
Sst
Pvalb
Meis2
L2/3 IT
L4 IT
L5 IT
L6 IT
L5 PT
L6 CT
L6b
CR
Astro
Oligo
VLMC
Endo
Peri
Macro

Figure S2. Comparison of scATAC-seq with scRNA-seq for same transgenic lines, related to Figure 2. To assess the accuracy of our scATAC-seq mapping to transcriptomic subclasses, we examined driver lines for which we collected both scATAC-seq and scRNA-seq data (the latter from Tasic *et al.* (Tasic et al., 2018)). For each combination of driver and reporter mouse line, we show the number of samples obtained for each method (scATAC-seq or scRNA-seq) and plot the fraction of cells assigned to each group used in **Fig. 2** as colored bars for each method. Differences in proportions may be due to differences in dissection and region sampling strategies. Gray hashed bars indicate that no cells were assessed by scRNA-seq for specific driver and reporter line combinations.

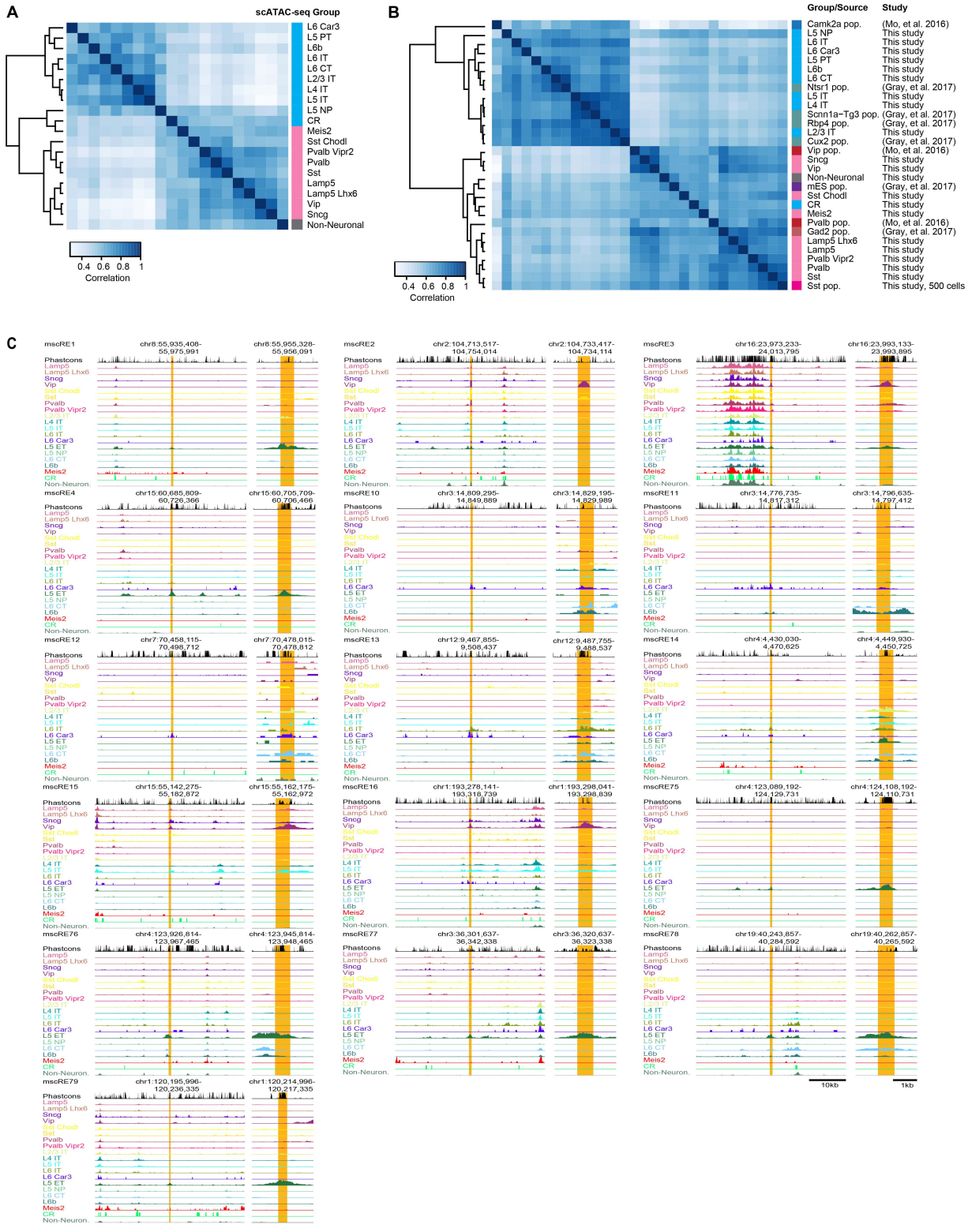
A
scATAC-seq Group
L6 Car3
L5 PT
L6b
L6 IT
L6 CT
L2/3 IT
L4 IT
L5 IT
L5 NP
CR
Meis2
Sst Chodl
Pvalb Vipr2
Pvalb
Sst
Lamp5
Lamp5 Lhx6
Vip
Sncg
Non-Neuronal
0.4 0.6 0.8 1
Correlation
B
Group/Source
Study
Camk2a pop. (Mo, et al. 2016)
L5 NP This study
L6 IT This study
L6 Car3 This study
L5 PT This study
L6b This study
L6 CT This study
Ntsr1 pop. (Gray, et al. 2017)
L5 IT This study
L4 IT This study
Scnn1a−Tg3 pop. (Gray, et al. 2017)
Rbp4 pop. (Gray, et al. 2017)
L2/3 IT This study
Cux2 pop. (Gray, et al. 2017)
Vip pop. (Mo, et al. 2016)
Sncg This study
Vip This study
Non-Neuronal This study
mES pop. (Gray, et al. 2017)
Sst Chodl This study
CR This study
Meis2 This study
Pvalb pop. (Mo, et al. 2016)
Gad2 pop. (Gray, et al. 2017)
Lamp5 Lhx6 This study
Lamp5 This study
Pvalb Vipr2 This study
Pvalb This study
Sst This study
Sst pop. This study, 500 cells
0.4 0.6 0.8 1
Correlation
C
mscRE1 chr8:55,935,408-55,975,991 chr8:55,955,328-55,956,091
mscRE2 chr2:104,713,517-104,754,014 chr2:104,733,417-104,734,114
mscRE3 chr16:23,973,233-24,013,795 chr16:23,993,133-23,993,895
mscRE4 chr15:60,685,809-60,726,366 chr15:60,705,709-60,706,466
mscRE10 chr3:14,809,295-14,849,889 chr3:14,829,195-14,829,989
mscRE11 chr3:14,776,735-14,817,312 chr3:14,796,635-14,797,412
mscRE12 chr7:70,458,115-70,498,712 chr7:70,478,015-70,478,812
mscRE13 chr12:9,467,855-9,508,437 chr12:9,487,755-9,488,537
mscRE14 chr4:4,430,030-4,470,625 chr4:4,449,930-4,450,725
mscRE15 chr15:55,142,275-55,182,872 chr15:55,162,175-55,162,972
mscRE16 chr1:193,278,141-193,318,739 chr1:193,298,041-193,298,839
mscRE75 chr4:123,089,192-124,129,731 chr4:124,108,192-124,410,731
mscRE76 chr4:123,926,814-123,967,465 chr4:123,945,814-123,948,465
mscRE77 chr3:36,301,637-36,342,338 chr3:36,320,637-36,323,338
mscRE78 chr19:40,243,857-40,284,592 chr19:40,262,857-40,265,592
mscRE79 chr1:120,195,996-120,236,335 chr1:120,214,996-120,217,335
Phastcons
Lamp5
Lamp5 Lhx6
Sncg
Vip
Sst Chodl
Sst
Pvalb
Pvalb Vipr2
L2/3 IT
L4 IT
L5 IT
L6 IT
L6 Car3
L5 ET
L5 NP
L6 CT
L6b
Meis2
CR
Non-Neuron.
10kb
1kb

Figure S3. Comparison of our dataset with existing datasets and all mscREs (16 total) examined in this study, related to Figure 3. (**A**) Pairwise correlations between select cell classes, subclasses, and types defined by clustering scATAC-seq data in this study using the DiffBind package for R (Stark and Brown, 2011) (**STAR Methods**) show expected grouping of GABAergic and glutamatergic cell subclasses and types. The heatmap shows weighted pairwise correlations between each pair of aggregated scATAC-seq cell populations. (**B**) Approach in (A) was used to compare scATAC-seq clusters with population ATAC-seq datasets generated by Mo *et al.* (Mo et al., 2015), Gray *et al.*, (Gray et al., 2017), or in this study (Sst pop. – "pop." indicates that the data were experimentally obtained from a population of cells, and not from single cells). Expected divisions and groupings are observed. (**C**) Chromatin accessibility in clusters based on single cell ATAC-seq data for select genomic regions containing mscREs defined and examined in this study.

A

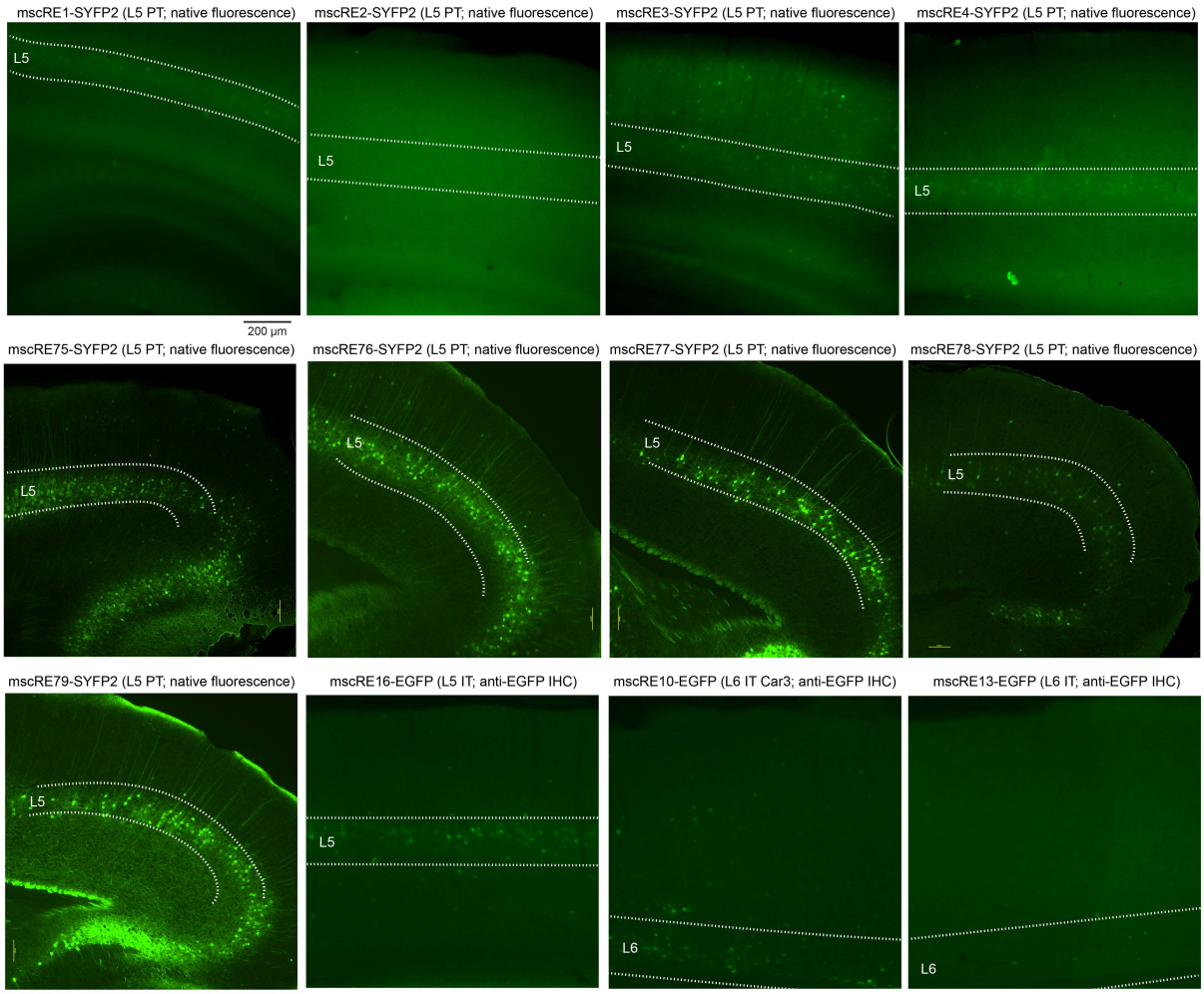

B

Number	Target cell subclass/type	mscRE	Shown in Fig S4A?	Desired layer enrichment?	Efficiency of desired labeling based on layer enrichment	Desired morphology observed?	Efficiency of desired labeling based on morphology	Transcriptionally confirmed (scRNA-seq and/or RNAscope)?	Efficiency of desired labeling based on transcriptional analysis	Efficiency of desired labeling based on modalities: layer enrichment (L), morphology (M) or transcriptional analysis (T)
1	L5 PT	mscRE1	Y	Y	7/9 (78%)	Y	7/9 (78%)	Y	2/2 (100%)	7/9 (78% for L, M)
2	L5 PT	mscRE2	Y	N		N		NE		
3	L5 PT	mscRE3	Y	N		N		NE		
4	L5 PT	mscRE4	Y	Y		Y		Y		
5	L5 PT	mscRE75	Y	Y		Y		NE		
6	L5 PT	mscRE76	Y	Y		Y		NE		
7	L5 PT	mscRE77	Y	Y		Y		NE		
8	L5 PT	mscRE78	Y	Y		Y		NE		
9	L5 PT	mscRE79	Y	Y		Y		NE		
10	L5 IT	mscRE15	N	N	1/2 (50%)	NE	NE	NE	1/1 (100%)	1/2 (50% for L, T)
11	L5 IT	mscRE16	Y	Y		NE	NE	Y		
12	L6 IT Car3	mscRE10	Y	Y	1/3 (33%)	NE	NE	N	0/1 (0%)	0/3 (0% for L,T)
13	L6 IT Car3	mscRE11	N	N		NE	NE	NE		
14	L6 IT Car3	mscRE12	N	N		NE	NE	NE		
15	L6 IT	mscRE13	Y	Y	1/2 (50%)	NE	NE	Y	1/1 (100%)	1/2 (50% for L, T)
16	L6 IT	mscRE14	N	N		NE	NE	NE		

Key
Y: yes; **N**: no;
NE: not evaluated

Figure S4. Initial screening of mscREs driving SYFP2 or EGFP, related to Figure 4. (**A**) Candidate enhancers were first tested by retro-orbital injection of direct fluorophore-expressing viruses. Epifluorescence images are shown of native fluorescence or antibody-enhanced (anti-GFP) fluorescence from VISp of C57BL/6J animals infected with virus. Dashed lines indicate the cortical layer expected to contain virus-labeled cells. mscRE1-4 were screened using self-complementary AAVs (scAAV) driving SYFP2 delivered at 1.0E+11 GC into P62 mice, whereas mscRE75-79 were screened using rAAVs driving SYFP2 delivered at 6.0-9.0E+11 GC into P36 mice. Enhancer viruses that exhibited no fluorescence (native or antibody-enhanced) in the initial screen were not included. (**B**) Summary of the results from the primary enhancer virus screen. Success rates were calculated based on the efficiency of labeling for each data modality (layer enrichment, morphology, and transcriptomics) and were grouped by subclass or type. The overall success rates are based on the labeling results obtained from either all three or at least two data modalities (yellow column). For more detailed descriptions of viral constructs, see **Table S5** and the **Key Resources Table**. For a general summary of all results, see **Table S8**.

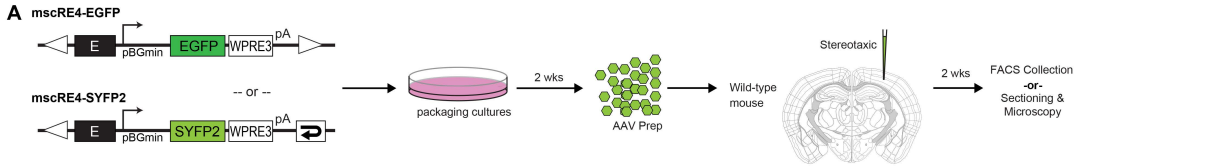
A
mscRE4-EGFP
E
pBGmin
EGFP
WPRE3
pA
-- or --
mscRE4-SYFP2
E
pBGmin
SYFP2
WPRE3
pA
packaging cultures
2 wks
AAV Prep
Wild-type mouse
Stereotaxic
2 wks
FACS Collection
-or-
Sectioning & Microscopy

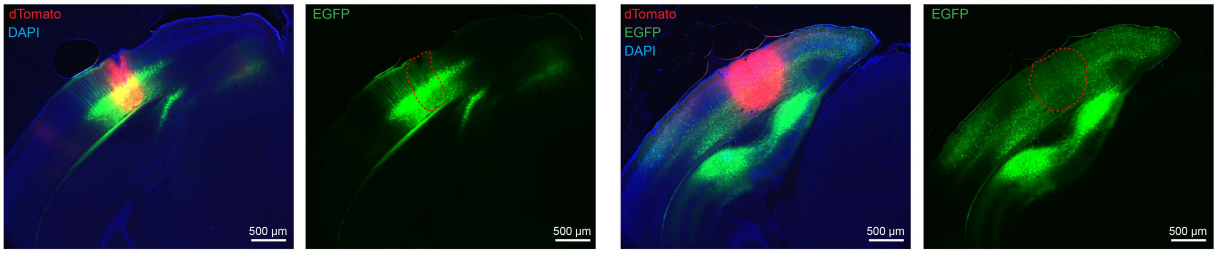
B Stereotaxic Injection (50 nL)
mscRE4-EGFP
dTomato
DAPI
EGFP
500 µm
C Stereotaxic Injection (250 nL)
mscRE4-EGFP
dTomato
EGFP
DAPI
EGFP
500 µm

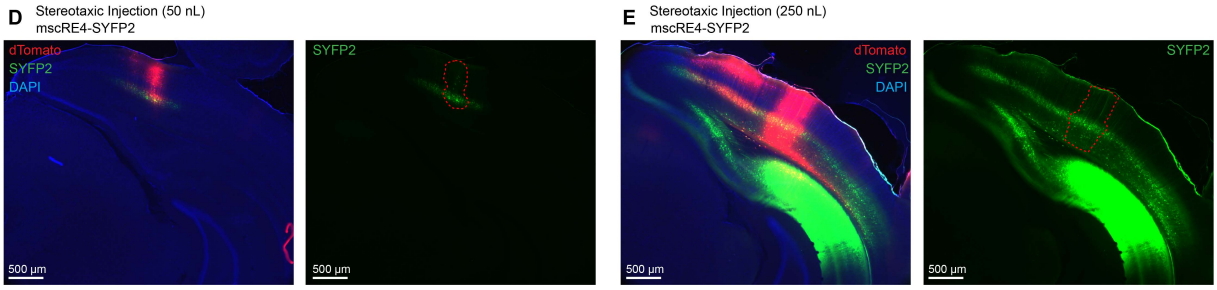
D Stereotaxic Injection (50 nL)
mscRE4-SYFP2
dTomato
SYFP2
DAPI
SYFP2
500 µm
E Stereotaxic Injection (250 nL)
mscRE4-SYFP2
dTomato
SYFP2
DAPI
SYFP2
500 µm

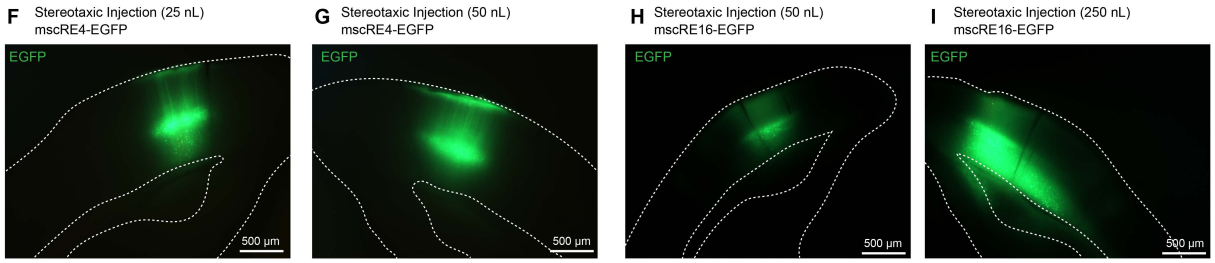
F Stereotaxic Injection (25 nL)
mscRE4-EGFP
EGFP
500 µm
G Stereotaxic Injection (50 nL)
mscRE4-EGFP
EGFP
500 µm
H Stereotaxic Injection (50 nL)
mscRE16-EGFP
EGFP
500 µm
I Stereotaxic Injection (250 nL)
mscRE16-EGFP
EGFP
500 µm

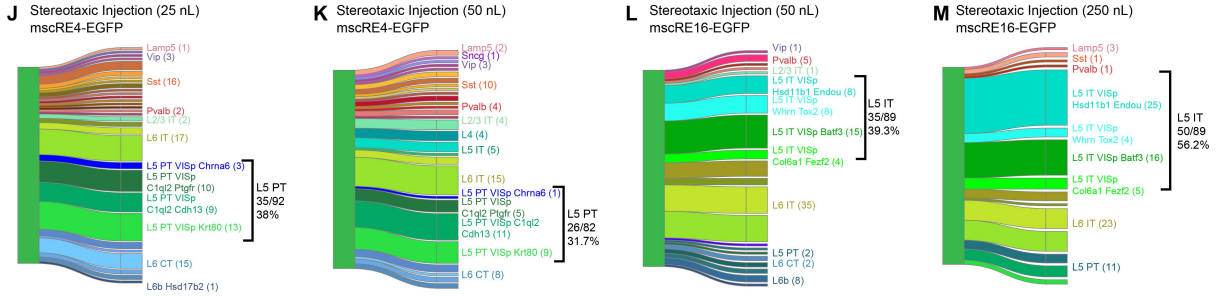
J Stereotaxic Injection (25 nL)
mscRE4-EGFP
Lamp5 (1)
Vip (3)
Sst (16)
Pvalb (2)
L2/3 IT (2)
L6 IT (17)
L5 PT VISp Chrna6 (3)
L5 PT VISp
C1ql2 Ptgfr (10)
L5 PT VISp
C1ql2 Cdh13 (9)
L5 PT VISp Krt80 (13)
L5 PT
35/92
38%
L6 CT (15)
L6b Hsd17b2 (1)
K Stereotaxic Injection (50 nL)
mscRE4-EGFP
Lamp5 (2)
Sncg (1)
Vip (3)
Sst (10)
Pvalb (4)
L2/3 IT (4)
L4 (4)
L5 IT (5)
L6 IT (15)
L5 PT VISp Chrna6 (1)
L5 PT VISp
C1ql2 Ptgfr (5)
L5 PT VISp C1ql2
Cdh13 (11)
L5 PT VISp Krt80 (9)
L5 PT
26/82
31.7%
L6 CT (8)
L Stereotaxic Injection (50 nL)
mscRE16-EGFP
Vip (1)
Pvalb (5)
L2/3 IT (1)
L5 IT VISp
Hsd11b1 Endou (8)
L5 IT VISp
Whrn Tox2 (8)
L5 IT VISp Batf3 (15)
L5 IT VISp
Col6a1 Fezf2 (4)
L5 IT
35/89
39.3%
L6 IT (35)
L5 PT (2)
L6 CT (2)
L6b (8)
M Stereotaxic Injection (250 nL)
mscRE16-EGFP
Lamp5 (3)
Sst (1)
Pvalb (1)
L5 IT VISp
Hsd11b1 Endou (25)
L5 IT VISp
Whrn Tox2 (4)
L5 IT VISp Batf3 (16)
L5 IT VISp
Col6a1 Fezf2 (5)
L5 IT
50/89
56.2%
L6 IT (23)
L5 PT (11)

Figure S5. Enhancer virus labeling by stereotaxic injection, related to Figure 4. (**A**) For stereotaxic injection, enhancer-driven fluorophore viruses were generated by cloning mscRE sequences in rAAV (EGFP viruses) or scAAV (SYFP2 virus) constructs. After packaging, purification, and titering, viruses were stereotaxically targeted to VISp into wild-type mice. (**B-C**) Native fluorescence imaging of animals with stereotaxic injection of mscRE4-EGFP in VISp at two injection volumes (50 nL and 250 nL). Enhancer-driven viruses were co-injected with a constitutively expressed dTomato virus, rAAVDJ-EF1a-dTomato, at 0.1X of the volumes of the mscRE viruses, to provide injection site location (red outlines). (**D-E**) Native fluorescence imaging of animals with stereotaxic injection of mscRE4-SYFP2 into primary visual cortex at two injection volumes (50 nL and 250 nL). The same injection site labeling strategy used in (A) was also utilized for these experiments. (**F-G**) Native fluorescence imaging of stereotaxic injections into the primary visual cortex using mscRE4-EGFP at 25 nL and 50 nL volumes injected into the left and right hemisphere, respectively. (**H-I**) as in (E-F) using mscRE16-EGFP at 50 nL and 250 nL volumes. (**J-M**) scRNA-seq mapping results for cells collected from panels above each river plot (e.g., cells in (I) were collected from the injections matching the conditions shown in (E) scRNA-seq data were mapped to a VISp cell type reference from Tasic *et al.* (Tasic et al., 2018). using a centroid classifier, and only cells that mapped to a single cluster in ≥ 80 of 100 bootstrapped classifications were retained for figures: (J) n = 92 of 96; (K) n = 82 of 96; (L) n = 89 of 96; and (M) n = 89 of 96.

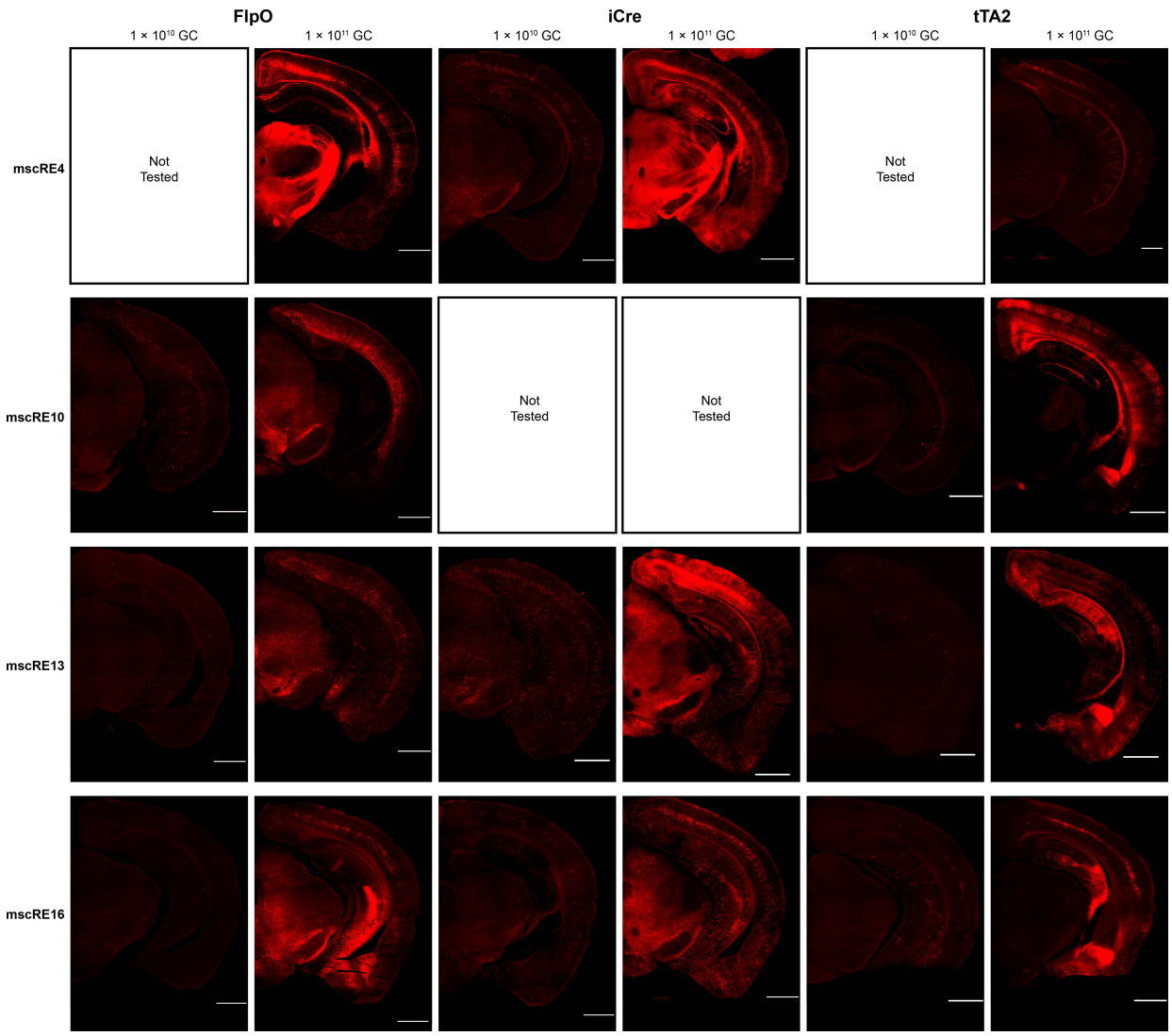
FlpO
iCre
tTA2
1 × 10^10 GC
1 × 10^11 GC
1 × 10^10 GC
1 × 10^11 GC
1 × 10^10 GC
1 × 10^11 GC
mscRE4
Not Tested
Not Tested
mscRE10
Not Tested
Not Tested
mscRE13
mscRE16

Figure S6. Labeling of retro-orbitally delivered mscRE viruses, related to Figure 5. Native fluorescence of tdTomato imaged in reporter mice injected retro-orbitally with enhancer-driven recombinase or tTA2; 1 $\times 10^{10}$ genome copies (GC) or 1×10^{11} GC of virus was delivered. Each enhancer is shown in a row, and each driver/reporter/dose combination is shown in a column. Reporter mouse lines used: *Ai65F* for FlpO, *Ai14* for iCre, and *Ai63* for tTA2. All scale bars (white) are 500 μm.


A mscRE1-SYFP2 Retro-orbital in wt
L6 IT VISp Col18a1
10 3 4 138
0 0
L5 PT VISp V1ql2 Ptgfr
21 3 22 70
0 0
L5 PT VISp C1ql2 Cdh13
11 0 6 84
0 0
B mscRE4-SYFP2 Retro-orbital in wt
L5 PT VISp V1ql2 Ptgfr
49 7 24 70
0 0
L5 PT VISp C1ql2 Cdh13
85 68 63 84
0 1
Cdkl1
L5 PT VISp Krt80
54 34 68 151
0 1
Egr1
C mscRE4-FlpO Retro-orbital in Ai65F
L5 PT VISp C1ql2 Ptgfr
56 451 656 70
0 0
L5 PT VISp C1ql2 Cdh13
55 533 616 84
0 0
L5 PT VISp Krt80
17 140 341 151
0 0
D mscRE10-FlpO Retro-orbital in Ai65F
L6 CT VISp Ctxn3 Brinp3
17 25 42 196
1 0
Egr1
L6 CT VISp Ctxn3 Sla
11 21 8 226
0 0
E mscRE16-FlpO Retro-orbital in Ai65F
Lamp5 Lsp1
11 92 26 450
0 0
F mscRE4-EGFP Stereotaxic in wt, 25 nL, 4.1 x 10⁹ GC
L6 IT VISp Col18a1
12 19 51 138
0 0
L5 PT VISp C1ql2 Cdh13
13 18 203 84
0 0
L5 PT VISp Krt80
10 43 205 151
0 0
G mscRE4-EGFP Stereotaxic in wt, 50 nL, 8.2 x 10⁹ GC
L6 IT VISp Col18a1
12 29 79 138
3 0
Isg15
Usp18
L5 PT VISp C1ql2 Cdh13
11 5 889 70
2 2
Isg15
L5 PT VISp Krt80
13 82 365 151
11 0
Isg15
Irf7
Bst2
Ifit1
Mx2
Irf9
Xaf1
Usp18
Stat1
H mscRE16-EGFP Stereotaxic in wt, 50 nL, 9.7 x 10⁹ GC
L5 IT VISp Batf3
17 85 280 361
0 0
L6 IT VISp Col23a1 Adamts2
12 35 39 296
0 0
L6 IT VISp Col18a1
12 16 80 138
0 0
I mscRE16-EGFP Stereotaxic in wt, 250 nL, 4.8 x 10⁹ GC
L5 IT VISp Hsd11b1 Endou
25 158 546 181
13 0
Isg15
Mx1
Irf7
Usp18
Bst2
Ifit1
Stat1
Irf9
Oas2
Isg20
L5 IT VISp Batf3
16 65 226 361
9 0
Isg15
Ifit1
Bst2
Usp18
Irf7
Oas2
L6 IT VISp Col23a1 Adamts2
10 76 92 296
5 0
Mx2
Usp18
Ifit1
Irf7
Legend
N genes higher in virus-labeled
N genes higher in driver-labeled
N virus-labeled samples
N transgenic driver-labeled samples
11
92
26
450
0
0
N innate immune genes higher in virus-labeled
N innate immune genes higher in driver-labeled
log10(p-value)
log2(Fold Change)

Figure S7. Differential gene expression induced by viral labeling, related to Figure 4 and S5. For each set of scRNA-seq data collected from virally labeled cells (**A–I**), we selected all cell types to which at least 10 cells were mapped. For each selected cell type, we performed pairwise differential gene expression analysis between virally labeled cells and cells labeled by transgenic recombinase driver mouse lines from Tasic *et al.* (Tasic et al., 2018) (**STAR Methods**). A volcano plot is shown for each comparison. Each gene is represented by a point. Log_2(fold change) is displayed on the x-axis, with genes higher in virally-labeled cells on the left and higher in transgenic mouse lines on the right. Log_{10}(adjusted p-value) is displayed on the y-axis. Significantly differentially expressed genes (adjusted p-value < 0.01) are highlighted in blue (higher in virally-labeled cells) and orange (higher in transgenic mouse lines). Differentially expressed innate immunity-related genes are highlighted in magenta. Counts for the number of cells in each group and the number of differentially expressed genes and immune-related genes are shown in each plot. The legend below panel (**H**) applies to all plots.

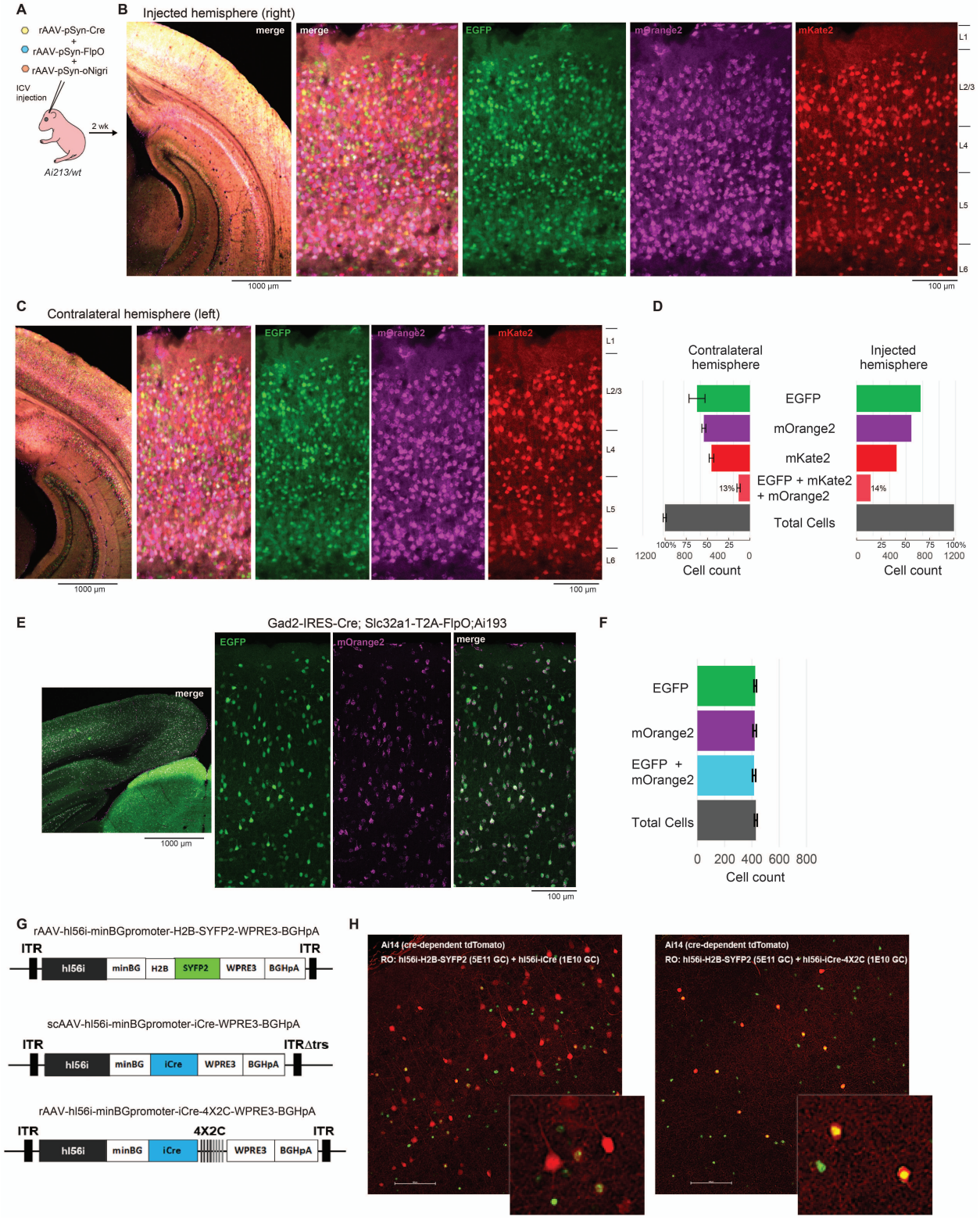
A
rAAV-pSyn-Cre
+
rAAV-pSyn-FlpO
+
rAAV-pSyn-oNigri
ICV injection
2 wk
Ai213/wt
B
Injected hemisphere (right)
merge
merge
EGFP
mOrange2
mKate2
L1
L2/3
L4
L5
L6
1000 µm
100 µm
C
Contralateral hemisphere (left)
EGFP
mOrange2
mKate2
L1
L2/3
L4
L5
L6
1000 µm
100 µm
D
Contralateral hemisphere
Injected hemisphere
EGFP
mOrange2
mKate2
EGFP + mKate2 + mOrange2
Total Cells
13%
14%
100% 75 50 25
1200 800 400 0
0 400 800 1200
Cell count
E
Gad2-IRES-Cre; Slc32a1-T2A-FlpO;Ai193
merge
EGFP
mOrange2
merge
1000 µm
100 µm
F
EGFP
mOrange2
EGFP + mOrange2
Total Cells
0 200 400 600 800
Cell count
G
rAAV-hl56i-minBGpromoter-H2B-SYFP2-WPRE3-BGHpA
ITR
hl56i
minBG
H2B
SYFP2
WPRE3
BGHpA
ITR
scAAV-hl56i-minBGpromoter-iCre-WPRE3-BGHpA
ITR
hl56i
minBG
iCre
WPRE3
BGHpA
ITRΔtrs
rAAV-hl56i-minBGpromoter-iCre-4X2C-WPRE3-BGHpA
ITR
hl56i
minBG
iCre
4X2C
WPRE3
BGHpA
ITR
H
Ai14 (cre-dependent tdTomato)
RO: hl56i-H2B-SYFP2 (5E11 GC) + hl56i-iCre (1E10 GC)
Ai14 (cre-dependent tdTomato)
RO: hl56i-H2B-SYFP2 (5E11 GC) + hl56i-iCre-4X2C (1E10 GC)

Figure S8. Increased labeling efficiency achieved with ICV injection of viruses or all transgenic strategy and new vector to target forebrain GABAergic neurons, related to Figure 7. (**A-C**) *Ai213/wt* animals at postnatal day 3 (P3) were injected with a mixture of the three pan-neuronal recombinase viruses each at 2.1 X 10^{10} GC into the right cerebral ventricle and reporter expression in the brain was analyzed two-weeks post-injection. (**D**) The labeled cells for each fluorophore alone or the combination of all three were counted in confocal images collected from primary visual cortex of ICV injected animals (n = 2). Quantification from both hemispheres is presented and shows a similar number of labeled cells in all groups between both regions. (**E**) Representative confocal images from VISp of a *Gad2-IRES-Cre/wt;Slc32a1-T2A-FlpO/wt;Ai213/wt* triple-transgenic animal. Pan-inhibitory labeling patterns were observed for both fluorophores with near perfect overlap of EGFP and mOrange2 when quantified (**F**). Data in bar graphs are mean ± S.E.M. (**G**) Diagram of AAV vector designs. Top vector: *DLX* hl56i enhancer driving a histone 2B-tagged SYFP2 fluorophore, Bottom left vector: hl56i enhancer driving iCre, Bottom right vector: hl56i enhancer driving iCre with 3' 4X2C mAGNET sequence to suppress excitatory neuron labeling (Sayeg et al., 2015). (**H**) Viruses were co-delivered (RO) into *Ai14* mice at the doses indicated and native tdTomato (red) and SYFP2 (green) fluorescence was evaluated in micrographs from adult mouse neocortex. Labeling of both excitatory and inhibitory populations was observed with hl56i-iCre virus (left panel), compared to exclusively GABAergic cell type labeling with hl56i-iCre-4X2C virus (right panel). Scale bars,100 microns.